Abstract

In this master thesis an investigation of a buoyancy-driven boundary layer has been done. This kind of flow is very hard to predict numerically, because of limitations of the turbulence models used, which in turn is caused by the lack of of accurate and detailed measurements. An experiment is proposed to provide new data on the buoyancy-driven turbulent boundary layer, where particular attention is given to the near-wall region. This experiment will both work as a validation for numerical codes as well as shed new light on the physics behind the phenomena. The experimental rig will be built up at the division of Thermo and Fluid Dynamics at Chalmers University of Technology.

The first task of the project was to make a literature review of recent experimental work and of the underlying theories for buoyancy-driven boundary layers. The review of experimental work confirmed that the lack of detailed experimental data for turbulent natural convection flows at high Grashof numbers, and that the proposed experimental methodology for simultaneous measurements of velocity and temperature is appropriate. An investigation of the inlet flow into the proposed experimental facility showed large deviations from the desired inlet conditions of axisymmetric radial inflow. The recommendation was therefore to redesign the inlet and improve the contraction in order to satisfy the requirement on the inlet flow. The second task was to investigate the turbulent structures in this flow. To do this, data from a direct numerical simulation (DNS) was used. Two techniques were used for the investigation, the first to identify vortex structures based on a modification of pressure minimum definition. The second technique used was based on proper orthogonal decomposition (POD). A variant called "snapshot POD" was used here.

From the analysis of the coherent structures it was found that, so called horseshoe vortices exist in the flow. From the "snapshot POD" it was found that the first modes only contained about 7-9 % of the energy. This is low compared to what has been reported for other flow cases. The most probable explanations are that either too few samples were used, or that the cyclic boundary conditions in the simulations affected the result. In the latter case, POD would transform to Fourier decomposition, in which case many modes are necessary to comprise the field.

Acknowledgements

This master thesis has been carried out at the division of Thermo and Fluid Dynamics, Chalmers University of Technology, Gothenburg, Sweden.

I would like to thank my examiner, adjunct Professor Rolf Karlsson, and my supervisor, assistant Professor Peter Johansson, for all help and great discussions during this project.

I also like to express my gratitude to Professor William K George and associate Professor Gunnar Johansson for always having time to answer my questions and for a great work with the IMP in Turbulence.

Further, Professor Lars Davidson and Ph.D. student Darioush Gohari Barhaghi are gratefully acknowledged for providing me the DNS data used for this project.

Thanks also to Carlos Arroyo and Elteyeb Eljack for the nice discussions and collaboration.

Finally, I want to thank my parents, Lars and Marianne, for always supporting and encouraging me.

Nomenclature

Latin

$\mathbf{A}$	Matrix containing all $\mathbf{b}_l$ [-]
A	Element in the coefficient matrix [-]
b_k	Coefficient of POD mode k [-]
$\mathbf{b}_l$	POD coefficient vector [-]
c_p	Specific heat at constant pressure $[\frac{J}{kgK}]$
$\mathbf{C}$	Correlation matrix [-]
D	Depth of computational geometry [-]
f	Function of [-]
F_0	Kinematic wall heat flux $[\frac{mK}{s}]$
g	Gravitational force $[\frac{m}{s^2}]$
H	Height of computational geometry [-]
H_c	Height of contraction [m]
H_1	Height of contraction inlet [m]
H_2	Height of contraction outlet [m]
k	Thermal conductivity $[\frac{W}{mK}]$
L	Streamwise length scale [m]
L_c	Length of contraction [m]
m	Number of velocity components [-]
n	Spanwise spatial position [-]
N	Total number of realizations [-]
o	Streamwise spatial position [-]
p	Fluctuating pressure [Pa]
P	Mean pressure [Pa]
$P_\star$	Mean static pressure minus hydrodynamic pressure [Pa]
q_w	Wall heat flux $[\frac{W}{m^2}]$
r	Radial coordinate [m]
r_c	Radial coordinate for contraction [m]
r_m	Matching point for contraction [m]
$\mathbf{R}$	Two-point correlation function $[\frac{m^2}{s^2}]$
S	Strain rate tensor $[\frac{1}{s}]$
t	Time [s]
T	Stress tensor $[\frac{1}{s}]$

$u_\star$	$= \sqrt{\frac{\tau_w}{\rho}}$ Friction velocity $[\frac{m}{s}]$
$\mathbf{v}$	Velocity vector $[\frac{m}{s}]$
V	Volume $[m^3]$
v_r	Radial fluctuating velocity $[\frac{m}{s}]$
v_x	Streamwise fluctuating velocity $[\frac{m}{s}]$
v_y	Cross-stream fluctuating velocity $[\frac{m}{s}]$
v_z	Spanwise fluctuating velocity $[\frac{m}{s}]$
V_r	Mean radial velocity $[\frac{m}{s}]$
V_x	Mean streamwise velocity $[\frac{m}{s}]$
V_y	Mean cross-stream velocity $[\frac{m}{s}]$
V_z	Mean spanwise velocity $[\frac{m}{s}]$
W	Width of computational geometry [-]
$\mathbf{x}$	Space vector [m]
x	Streamwise coordinate [m]
y	Spanwise coordinate [m]

Greek symbols

α	Thermal diffusivity $[\frac{m^2}{s}]$
β	$= \left[-\frac{1}{\rho}\left(\frac{\partial\tilde{\rho}}{\partial\tilde{\Theta}}\right)_{p=contant}\right]_\infty$ Thermal expansion coefficient $[\frac{1}{K}]$
δ	Outer cross-stream length scale [m]
δ_{ij}	Kronecker delta [-]
ΔP	Pressure difference [Pa]
η	Inner cross-stream length scale [m]
η_t	Inner thermal cross-stream length scale [m]
θ	Azimuthal coordinate [rad]
θ	Fluctuating temperature [K]
Θ	Mean temperature [K]
λ	Eigenvalue [-]
μ	Dynamic viscosity $[\frac{Ns}{m^2}]$
ν	Kinematic viscosity $[\frac{m^2}{s}]$
ρ	Mean density $[\frac{kg}{m^3}]$
ρ'	Fluctuating density $[\frac{kg}{m^3}]$
τ_w	Wall shear stress $[\frac{N}{m^2}]$
$\boldsymbol{\phi}$	Deterministic vector field [-]
$\mathbf{\Phi}$	Basis modes [-]
$\mathbf{\Phi}$	Dissipation function $[\frac{N}{m^2 s}]$
$\mathbf{\Psi}$	Vector of basis modes [-]
Ω	Region in space [-]
Ω	Rotation tensor $[\frac{1}{s}]$

Non-dimensional parameters

Gr	$= \frac{g\beta(\Theta_w - \Theta)L^3}{\nu^2}$ The Grashof number
H	$= Gr \times Nu \times Pr^2$ The "H-number"
Nu	$= \frac{hL}{k}$ The Nusselt number
Pe	$=$ Re$\times$Pr The Peclet number
Pr	$= \frac{\nu}{\alpha}$ The Prandtl number
Ra	$=$ Pr$\times$Gr The Rayleigh number
Re	$= \frac{VL}{\nu}$ The Reynolds number

Overlines

$\bar{}$	Averaged quantities
$\tilde{}$	Instantaneous quantities
$\hat{}$	Discrete quantities

Subscripts

i,j,k	Indices for tensor notation
k,l	Indices of realization number
Si	Scaling functions for inner variables
So	Scaling functions for outer variables
w	Evaluated at the wall
x	Based on a vertical length scale
∞	Evaluated at infinite distance from the wall

Superscripts

$*$	Complex conjugate
'	Another position
T	Transpose

Relation symbols

$\sim$	"on the order of magnitude of"
$\equiv$	"defined as" (equivalent to)
$\cong$	"approximately equal to"
$\propto$	"proportional to"

Abbreviations

DNS	Direct Numerical Simulation
HWA	Hot-Wire Anemometry
HVAC	Heat, Ventilation and Air Condition
LDA	Laser Doppler Anemometry
LES	Large Eddy Simulation
PIV	Particle Image Velocimetry
POD	Proper Orthogonal Decomposition

Contents

Chapter 1

Introduction

1.1 Background

Buoyancy-driven flows are important in many areas of application. They represent a fundamental problem in heat transfer research and occurs in many engineering situations. Examples of engineering applications where buoyancy-driven flows are present and play an important role are cooling of nuclear power plants, cooling of electronic devices, home heating and copper refining. They are also an important feature in the atmosphere, e.g. in the process of cloud formation and creation of tornados.

Buoyancy-driven flows appear when there is a density gradient. This density gradient is normally caused by chemical reactions or temperature differences. Buoyancy-driven flows can be either pure natural convection or some combination with forced convection, usually called mixed convection. The present work is restricted to buoyancy-driven boundary layer flows. Studies of buoyancy-driven boundary layers have been theoretical, experimental and numerical based on computer simulations. The investigations many times show different results. In chapter 2 a literature review is presented and it will be demonstrated that the investigations show different results.

The division of Thermo and Fluid Dynamics, Chalmers University of Technology has an on-going project that focus on Large Eddy Simulation (LES) of buoyancy affected flows. The proposed experimental set-up will work as a validation for these LES computations. The proposed experimental set-up is a modification of the one described in Persson and Karlsson (1996). More specifications, including a schematic picture, for the experimental set-up can be found in appendix B.

1.2 Objectives and methods

The purpose of the present work was to perform basic measurements of the flow for the proposed experimental set-up. Initial measurements of the inlet flows showed, however, a velocity variation around the perimeter of about $\pm 10\%$. Such a large variation was considered unacceptable (the axisymmetry condition was not satisfied) and the inlet section had to be redesigned. Measurement of the velocity for the initial contraction, together with drawing of a modified version of a new contraction, can be found in appendix C. The redesign and manufacturing of the new inlet section was time consuming and made further measurement impossible within the time frame of this master thesis. The focus of the work was therefore shifted towards an general investigation of this kind of flows, as a preparation for a future experiment. The first task was to perform a literature review of previous investigations. The second task was to investigate the turbulent structure of buoyancy-driven flows using Direct Numerical Simulation (DNS). Computer based visualization and a decomposition technique called Proper Orthogonal Decomposition, POD, have been chosen as tools for this part.

Chapter 2

Literature review

Buoyancy-driven boundary layers have been investigated for many years with varying degrees of success. In the beginning the focus was to perform single point measurements using thermal anemometry to measure velocity and temperature separately. The problem with thermal anemometry is that velocity measurements can not be made very accurately in flows with varying temperature. With the development of laser based methods that are capable of measuring velocity more accurately, independent of temperature variations, more reliable data was obtained. The rapid increase of computer capacity for the last decades has lead to that much work is spent on numerical simulations. This has in some ways shifted the focus from basic research to more applied studies.

In this chapter a review is presented of previous work most related to this study is presented. For more detailed reviews on buoyancy dominated flows, see Wosnik (1994). The chapter is divided into one section about previous experiments and another section about previous theoretical and numerical investigations. The conclusion of the review is that there is a great need to conduct new, refined experiments because of the discrepancies found in the previous investigations.

2.1 Previous experimental investigations

Cheesewright (1968) used used hot-wire anemometry (HWA) and resistance wires for measurements of velocities and temperatures of a turbulent natural convection along a heated vertical flat plate. This was considered to be the best experiment until Hoogendorn and Euser (1978) found that the energy balance was not satisfied in Cheesewrights experiment. Hoogendorn and Euser used hot-wires and thermo-couples for the velocity and temperature measurements, respectively. The problem when using HWA in turbulent natural convection flows is that the expected velocities in these flows are less than 1 m/s and that the HWA is sensitive to velocity and temperature simultaneously, which makes it difficult to separate velocity fluctuations from temperature fluctuations. For such small velocities is

the HWA very difficult to calibrate and the accuracy of measured results is poor.

Hoogendorn and Euser used a special low velocity anemometer for velocities below 0.3 m/s. Ierokipiotis (1983) used laser doppler anemometry (LDA) to measure the velocity. The main advantage of LDA compared to HWA in this case is that it gives accurate measurements for low velocities and it does not affect the flow, since it is a non-intrusive technique. Another challenge in this flow is to perform simultaneous measurements of velocity and temperature with high spatial resolution so both quantities can be considered to be measured in the same point. This is needed to obtain the physically and theoretically important velocity-temperature correlations. Miyamoto et al. (1982) used LDA and thermo-couples, while Tsuji and Nagano (1988a, b) used a combination of V-shaped hot-wires and resistance wires for this purpose. Tsuji et al. (1991) extended previous work to higher Grashof number. The Grashof number is a fundamental parameter that governs buoyancy-driven flows. More about it is given in chapter 3. They found that the Reynolds's stress, $\overline{v_x v_y}$, was positive all the way to the wall. On the other hand, Kato et al. (1993) found a region of negative $\overline{v_x v_y}$ using LDA for the velocity measurements. Persson and Karlsson (1996) also found a region of negative $\overline{v_x v_y}$ close to the wall, but they used a vertical cylinder instead of a vertical flat plate. They used LDA for the velocity measurements and a cold wire as resistance thermometer for the temperature measurements. There are uncertainties in to what extent the resistance wire affected the velocity measurement. Recent work on measurement technique for simultaneous measurements of velocity and temperature, of relevance for the present work, is reported by Heist and Castro (1998), Pietri et al. (2001) and Tagawa et al. (2001). In particular, Heist and Castro (1998) show that a larger physical distance between LDA measuring volume and thermometer is needed than that used by Persson and Karlsson(1996). Despite some uncertainty in the result, the measurements of Tsuji and Nagano are the ones often used to validate numerical simulations.

2.2 Theoretical and numerical investigation

The theoretical paper that is mostly cited is the paper by George and Capp (1979). They based their theory on similarity analysis for infinite Grashof numbers. Wosnik and George (1994) extended that theory to treat finite Grashof numbers. Versteegh and Nieuwstadt (1998) used direct numerical simulation to investigate the natural convection between two vertical, differentially heated walls and quite low Grashof number. Their results were not in agreement with the asymptotic solution of George and Capp. This could have been anticipated given the low Grashof number. In particular, the important ratio of outer to inner length scales need to be at least 1000 for an asymptotic theory to be applicable. For the DNS it was lower than 100. Today, because of the increase in computer performance and that shorter time for product development is demanded, much work for these kind

of flows is spent on computational fluid dynamics (CFD). Examples are Camargo et al. (1996), Barhaghi et al. (2002) and Davidson et al. (2003). Computations often rely on theoretical and experimental investigations. Because of the uncertainties mentioned in the previous section, the computations do not predict accurate results, especially close to walls. This is why it is important to conduct new experiments of the turbulent natural convection boundary layer next to walls with the improved experimental techniques that are now available.

Chapter 3

Theory for buoyancy-driven boundary layers

The aim of this chapter is to provide a theoretical background to buoyancy-driven boundary layer flows next to a vertical surface, including the governing equations. Most focus will be put on pure natural convection, but mixed convection will also be treated. A discussion about heat transfer features will also be given. The derivation of the governing equations follows Wosnik (1994). The approximations that are made to achieve the equations are of interest and should be verified in the proposed experiment.

3.1 Turbulent natural convection

Natural convection belongs to a class of flows that are called buoyancy-driven flows. Natural convection flows are caused by the density variations, most frequently related to temperature differences or chemical reactions, together with the acceleration of gravity. In the proposed experiment an internal cylinder wall is maintained at a constant temperature, which is higher than the surrounding temperature. The fluid will start to move from the bottom and form a laminar boundary layer. When the fluid is moving farther up along the wall the boundary layer will evolve into a transition region and finally it will become turbulent and ultimately, provided that the cylinder is long enough, fully turbulent.

The parameter that governs natural convection flow is the Grashof number defined as

$$Gr_L \equiv \frac{g\beta(\Theta_w - \Theta)L^3}{\nu^2} \tag{3.1}$$

where g is the acceleration of gravity, ν is the kinematic viscosity, $\Theta_w - \Theta$ is the difference between the local temperature and that at the wall, β is the thermal expansion coefficient and L is a length scale (often chosen as the vertical distance along the wall).The Grashof number can be interpreted as a ratio between

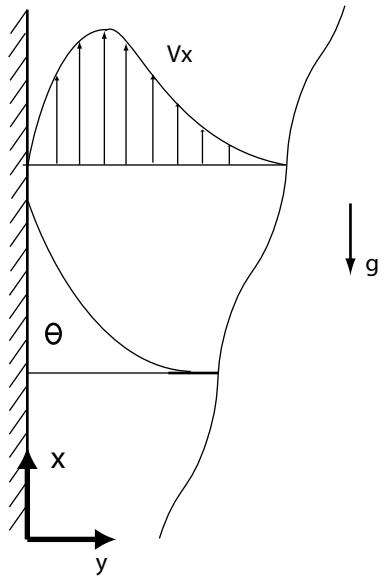

Figure 3.1: *A schematic picture of the turbulent natural convection boundary layer next to a heated wall with the coordinate system shown.*

buoyant forces and viscous forces and is based on a vertical length scale. Another parameter of interest is the Rayleigh number, which is simply $Ra_L = \mathrm{Pr}{\times}Gr_L$. Pr is the Prandtl number defined as ν/α. The transition from laminar to turbulent flow occur around $Gr_L \simeq 10^9$. Critical values of Gr_L ranging from $3.5{\times}10^8$ to $1.5{\times}10^{10}$ have been reported for air flows (Wosnik 1994). A schematic picture of the natural convection along a vertical wall is shown in figure 3.1.

Turbulent flows often arise from laminar flows as the Reynolds number (or the Grashof/Rayleigh number as in the case of natural convection) is increased. This is because small disturbances to the flow are not damped out by the flow and instead begin to grow by taking energy from the original laminar flow. One have to notice that there are two critical Grashof numbers. The first is when the flow becomes unstable at the first time and the second when the flow becomes fully turbulent. There is no exact definition of turbulence but there are some general characteristics of turbulent flows (Tennekes and Lumley (1972)).

- Turbulent flows are irregular and have a three-dimensional spatial character.
- Turbulent flows are very dissipative, which means that the kinetic energy is transferred from large scales to small scales and then finally transformed into internal energy.
- Turbulent flows are diffusive which give rise to an increase in mass, momentum and heat transfer.
- Turbulence occurs at high Reynolds numbers or as in the case with turbulent natural convection, high Grashof/Rayleigh numbers.

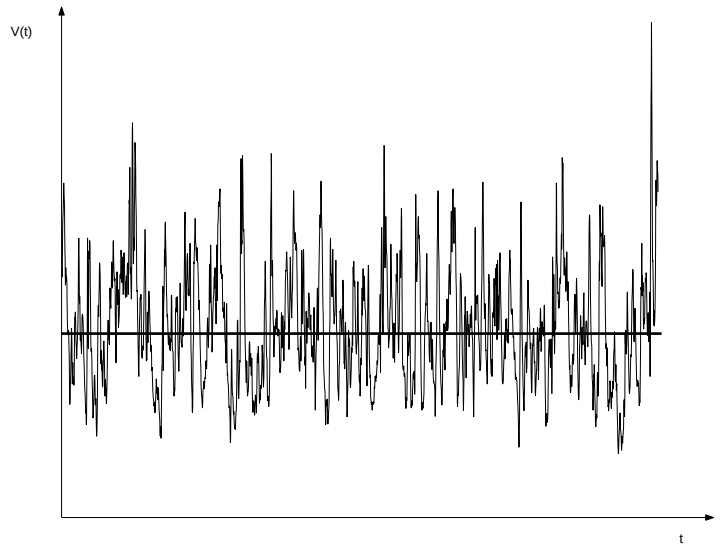

Figure 3.2: *A turbulent velocity signal as function of time. The straight line is the average value.*

- Turbulence is a continuum, which means that the smallest turbulent scales are much larger than the molecular size.
- Turbulence is not a feature of the fluid but of the fluid flow.

In figure 3.2 is a turbulent velocity signal shown as function of time. The straight line showing the average value.

3.2 Governing equations

Below are the instantaneous governing equations (continuity, momentum and energy) given in Cartesian tensor notation.

Equation of continuity

$$\frac{\partial \widetilde{\rho}}{\partial t} + \frac{\partial \widetilde{\rho}\widetilde{V_i}}{\partial x_i} = 0 \tag{3.2}$$

Equation of momentum

$$\widetilde{\rho}\left[\frac{\partial \widetilde{V_i}}{\partial t} + \widetilde{V_j}\frac{\partial \widetilde{V_j}}{\partial x_j}\right] = -\frac{\partial \widetilde{P}}{\partial x_i} + \frac{\partial \widetilde{T_{ij}}}{\partial x_j} + \widetilde{\rho} g_i \tag{3.3}$$

Equation of energy

$$\widetilde{\rho} c_p \left[\widetilde{V_j}\frac{\partial \widetilde{\Theta}}{\partial x_j} + \frac{\partial \widetilde{\Theta}}{\partial t}\right] - \beta\widetilde{\Theta}\left[\frac{\partial \widetilde{p}}{\partial t} + V_j\widetilde{\frac{\partial \widetilde{p}}{\partial x_j}}\right] = \frac{\partial}{\partial x_j}\left(k\frac{\partial \widetilde{\Theta}}{\partial x_j}\right) + \mathbf{\Phi} \tag{3.4}$$

where

$$\widetilde{T_{ij}} = 2\mu \left[\widetilde{S_{ij}} - \frac{1}{3}\widetilde{S_{kk}}\delta_{ij} \right] \tag{3.5}$$

$$\widetilde{S_{ij}} = \frac{1}{2} \left[\frac{\partial \widetilde{V_i}}{\partial x_j} + \frac{\partial \widetilde{V_j}}{\partial x_i} \right] \tag{3.6}$$

$$\beta \equiv \left[-\frac{1}{\tilde{\rho}} \left(\frac{\partial \tilde{\rho}}{\partial \tilde{\Theta}} \right)_{p=contant} \right]_{\infty} \tag{3.7}$$

and $\mathbf{\Phi}$ is the dissipation function, δ_{ij} is the Kronecker delta and β is the volumetric coefficient of thermal expansion.

To make it easier to handle, e.g. using statistically analysis, the instantaneous quantities can be divided into two parts, a mean and a fluctuating part. This decomposition is called *Reynolds decomposition* (Panton 1996). Reynolds decomposition is performed on pressure, density, temperature and velocities as shown below:

$\widetilde{P} = P + p$

$\widetilde{\rho} = \overline{\rho} + \rho$

$\widetilde{\Theta} = \Theta + \theta$

$\widetilde{V_i} = V_i + v_i$

where a capital letter means mean quantities and a lower case letter means fluctuating quantities, except for density where mean density is denoted by an overbar. The above quantities are dependent on both time and position. The mean quantities are ensemble averages and, for example in case of V_i, defined as

$$V_i(x, y, z, t) \equiv \lim_{N \to \infty} \frac{1}{N} \sum_{n=1}^{N} \widetilde{V_i}^{(n)}(x, y, z, t) \tag{3.8}$$

'N' is the total number of independent experiments. The other average quantities are defined in similar ways. It should be noted that an ensemble average is impossible to achieve during laboratory work. The governing equations 3.2-3.4 can be simplified. If the flow is assumed to be statistically stationary in time, these ensemble averages can be replaced by time averages.

Further, the dissipation function can normally be neglected. This can be done because the expected velocities are small and the temperature differences are not.

These equations can be even more simplified if assuming that the flow can be treated as incompressible. Flows that have large length scales, e.g. natural convection flow phenomena in the atmosphere, can not be treated as incompressible. For the experiment in this project, with a moderate length scale, it is a suitable assumption that the pressure can be treated as incompressible (Wosnik 1994). Using above assumptions, the equations 3.2-3.4 become:

Equation of continuity

$$\frac{\partial \widetilde{V}_i}{\partial x_i} = 0 \tag{3.9}$$

Equation of momentum

$$\tilde{\rho}\tilde{V}_j \frac{\partial \tilde{V}_i}{\partial x_j} = -\frac{\partial \tilde{p}}{\partial x_i} + \frac{\partial}{\partial x_j}\left(\mu \frac{\partial \tilde{V}_i}{\partial x_j}\right) + g_i \tilde{\rho} \tag{3.10}$$

Equation of energy

$$\widetilde{\rho} c_p \widetilde{V}_j \frac{\partial \widetilde{\Theta}}{\partial x_j} = \frac{\partial}{\partial x_j}\left(k \frac{\partial \widetilde{\Theta}}{\partial x_j}\right) \tag{3.11}$$

To account for temperature dependence of density the gradient of the hydrostatic pressure distribution can be written as:

$$\left(\frac{\partial \tilde{P}}{\partial x_i}\right)_{y\to\infty} = \frac{\partial P_\infty}{\partial x_i} = \rho_\infty g_i \tag{3.12}$$

P_∞ is the hydrostatic pressure at infinite distance from the wall. If assuming that the density can be treated as constant everywhere except where it appears in the body force, the Boussinesq assumption (Incropera 1995), the equation of momentum becomes

$$\tilde{V}_j \frac{\partial \tilde{V}_i}{\partial x_j} = -\frac{1}{\rho_\infty}\frac{\partial (P_\star + p)}{\partial x_i} + \frac{\partial}{\partial x_j}\left(\mu \frac{\partial \tilde{V}_i}{\partial x_j}\right) + g_i \frac{\tilde{\rho} - \rho_\infty}{\rho_\infty} \tag{3.13}$$

where $P_\star$ is the mean static pressure minus the hydrostatic pressure. The fluctuating pressure can be expanding in a Taylor series to relate the density to temperature. If neglecting higher order terms, the linearization becomes

$$\tilde{\rho} - \rho_\infty \approx -\rho_\infty \beta (\tilde{\Theta} - \Theta_\infty) \tag{3.14}$$

where the volumetric coefficient of thermal expansion, eguation 3.7, has been used again. If applying this linearization and averaging it will lead to the following set of equations.

Equation of continuity

$$\frac{\partial V_i}{\partial x_i} = 0 \tag{3.15}$$

Equation of momentum

$$V_j \frac{\partial V_i}{\partial x_j} = -\frac{1}{\rho_\infty}\frac{\partial P_\star}{\partial x_i} + \frac{\partial}{\partial x_j}\left(\nu \frac{\partial V_i}{\partial x_j} - \overline{v_i v_j}\right) - g_i \beta(\Theta - \Theta_\infty)\delta_{i1} \tag{3.16}$$

Equation of energy

$$V_j \frac{\partial \Theta}{\partial x_j} = \frac{\partial}{\partial x_j}\left(\alpha \frac{\partial \Theta}{\partial x_j} - \overline{v_j \theta}\right) \tag{3.17}$$

Note that the operations of averaging and differentiation commute. The linearization is not a good approximation for large temperature differences, but for moderate differences it is a suitable approximation.

3.3 The Reynolds' stress equation

An equation for the fluctuating velocities can be obtained by subtracting the momentum equation for the mean motion from the equation for the instantaneous motion.

$$V_j \frac{\partial v_i}{\partial x_j} = -\frac{1}{\rho}\frac{\partial p}{\partial x_i} + \frac{\partial}{\partial x_j}(2\nu s_{ij}) - \left(v_j \frac{\partial v_i}{\partial x_j} - \overline{v_j \frac{\partial v_i}{\partial x_j}}\right) - v_j \frac{\partial V_i}{\partial x_j} + g\beta\theta\delta_{i1} \tag{3.18}$$

Multiplying this equation by v_k and averaging leads to

$$V_j \overline{v_k \frac{\partial v_i}{\partial x_j}} = -\frac{1}{\rho}\overline{v_k \frac{\partial p}{\partial x_i}} + \overline{v_k \frac{\partial}{\partial x_j}(2\nu s_{ij})} - \overline{v_k v_j \frac{\partial v_i}{\partial x_j}} - \overline{v_k v_j}\frac{\partial V_i}{\partial x_j} + g\beta\theta\delta_{i1} \tag{3.19}$$

Rewriting this equation with reversed indexes i and k, adding both equations and rearranging leads to an equation for $\overline{v_k v_i}$

$$\begin{aligned} V_j \frac{\partial \overline{v_k v_i}}{\partial x_j} &= \frac{\partial}{\partial x_j}\left[\frac{1}{\rho}(\overline{v_i p}\delta_{kj} + \overline{v_k p}\delta_{ij}) - \overline{v_i v_k v_j} + 2\nu(\overline{v_k s_{ij}} + \overline{v_i s_{kj}})\right] \\ &+ \overline{\frac{p}{\rho}\left(\frac{\partial v_i}{\partial x_k} + \frac{\partial v_k}{\partial x_i}\right)} - \left(\overline{v_i v_j}\frac{\partial V_k}{\partial x_j} + \overline{v_k v_j}\frac{\partial V_i}{\partial x_j}\right) \\ &- 4\nu\overline{s_{ij}s_{kj}} + g\beta(\overline{v_k\theta}\delta_{i1} + \overline{v_i\theta}\delta_{k1}) \end{aligned} \tag{3.20}$$

This is the Reynolds' stress equation. If the free indices i and k are contracted it will give the equation for the turbulent kinetic energy.

$$\begin{aligned} V_j \frac{\partial(\frac{1}{2}\overline{v_i v_i})}{\partial x_j} &= \frac{\partial}{\partial x_j}\left[\frac{1}{\rho}\overline{v_j p} + 2\nu(\overline{v_i s_{ij}}) - \frac{1}{2}\overline{v_i v_i v_j}\right] \\ &- 2\nu(\overline{s_{ij}s_{ij}}) - \overline{v_i v_j}S_{ij} + g\beta\overline{v_i\theta}\delta_{i1} \end{aligned} \tag{3.21}$$

On the left-hand side is the convection of turbulent kinetic energy. The first three terms on the right-hand side are transport terms due to pressure-gradient work, viscous stresses and by velocity fluctuations, respectively. The fourth term is the viscous dissipation of turbulent kinetic energy. The fifth term is the turbulence production and the sixth term is the buoyant production.

In a similar way, an equation governing the transport of mean square temperature fluctuations can be derived. Subtracting the mean energy equation from the instantaneous equation, multiplying with the fluctuating temperature θ and averaging leads to

$$V_j \frac{\partial}{\partial x_j}\left(\frac{1}{2}\overline{\theta^2}\right) = \frac{\partial}{\partial x_j}\left[-\frac{1}{2}\overline{v_j\theta^2} + \alpha\frac{\partial}{\partial x_j}\left(\overline{\theta^2}\right)\right] - \overline{v_j\theta}\frac{\partial \Theta}{\partial x_j} - \alpha\overline{\frac{\partial\theta}{\partial x_j}\frac{\partial\theta}{\partial x_j}} \quad (3.22)$$

3.4 Three parts of the boundary layer

The turbulent natural convection boundary layer next to a heated vertical wall can be divided into two regions, an inner and an outer region, according to George and Capp (1979) and Wosnik and George (1994). The inner layer can be divided into two parts, the buoyant sublayer and the conductive and thermo-viscous sublayer. A schematic picture of the boundary layer can be found in figure 3.3. In this section are the equations for the different sub-layers provided. The assumptions are that the flow is homogenous in the spanwise direction and that the average velocity in that direction is zero. Because of the cylindrical geometry for the proposed experimental set-up, the governing equations are given in cylindrical coordinates in appendix A. The x-direction is directed opposite to the gravitational force and the y-direction is the direction directed out from the the heated wall, as shown in figure 3.1.

Equation of continuity

$$\frac{\partial V_x}{\partial x} + \frac{\partial V_y}{\partial y} = 0 \quad (3.23)$$

Equation of momentum in cross stream direction

$$\rho\left(V_y\frac{\partial V_y}{\partial y} + V_x\frac{\partial V_y}{\partial y}\right) = \mu\left[\frac{\partial^2 V_y}{\partial y^2} + \frac{\partial^2 V_y}{\partial x^2}\right] - \frac{\partial P_\star}{\partial y} + \frac{\partial(\overline{-v_y^2})}{\partial y} + \frac{\partial(\overline{-v_y v_x})}{\partial x} \quad (3.24)$$

Equation of momentum in vertical direction

$$\rho\left(V_y\frac{\partial V_x}{\partial y} + V_x\frac{\partial V_x}{\partial x}\right) = \mu\left[\frac{\partial^2 V_x}{\partial y^2} + \frac{\partial^2 V_x}{\partial x^2}\right] - \frac{\partial P_\star}{\partial x} + \rho g_x(\Theta - \Theta_\infty) + \frac{\partial(\overline{-v_x^2})}{\partial x} + \frac{\partial(\overline{-v_y v_x})}{\partial y} \quad (3.25)$$

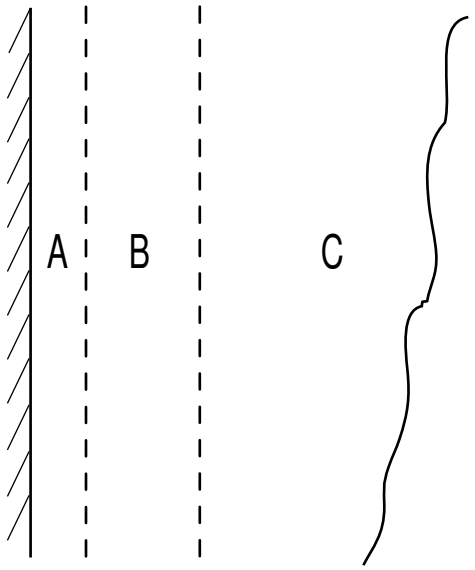

Figure 3.3: *The three parts of the turbulent natural convection boundary layer. A: The thermo-viscous and conductive sublayer. B: The buoyant sublayer. C: The outer region.*

Equation of momentum in spanwise direction

$$0 = \frac{\partial(\overline{-v_x v_z})}{\partial x} + \frac{\partial(\overline{-v_y v_z})}{\partial y} \tag{3.26}$$

Equation of energy

$$\rho c_p \left[V_y \frac{\partial \Theta}{\partial y} + V_x \frac{\partial \Theta}{\partial x} \right] = k \frac{\partial^2 \Theta}{\partial y^2} + k \frac{\partial^2 \Theta}{\partial x^2} + \frac{\partial(\overline{-v_y \theta})}{\partial y} + \frac{\partial(\overline{-v_x \theta})}{\partial y} \tag{3.27}$$

3.4.1 The outer region of the boundary layer

Further, the boundary layer approximation that $\partial/\partial x \sim 1/L \ll \partial/\partial y \sim 1/\delta$, where L is a streamwise and δ is a cross stream length scale, is applied and an order of magnitude analysis is performed (Tennekes and Lumley 1972). The mean velocities and temperature are scaled with V_{So} and Θ_{So} and the fluctuating velocities and temperature with v_{So} and θ_{So}. When doing the above steps the following set of equations are achieved

Equation of continuity

$$\frac{\partial V_x}{\partial x} + \frac{\partial V_y}{\partial y} = 0 \tag{3.28}$$

Equation of momentum in vertical direction

$$V_x\frac{\partial V_x}{\partial x}+V_y\frac{\partial V_x}{\partial y}\simeq-\frac{\partial\overline{(v_xv_y)}}{\partial y}+g\beta(\Theta-\Theta_\infty) \tag{3.29}$$

Equation of energy

$$V_x\frac{\partial\Theta}{\partial x}+V_y\frac{\partial\Theta}{\partial y}\simeq-\frac{\partial\overline{(\theta v_y)}}{\partial y} \tag{3.30}$$

with the following boundary conditions as y $\rightarrow\infty$

$$V_x=0 \tag{3.31}$$

$$\Theta=\Theta_\infty \tag{3.32}$$

$$-\overline{v_yv_x}=0 \tag{3.33}$$

$$-\overline{v_y\theta}=0 \tag{3.34}$$

The y-momentum equation has been used to eliminate the pressure term in the x-momentum equation. No viscous and conduction terms remain in the reduced equations 3.28-3.30. This imply that these equations are not valid close to the wall. A thing that is important to mention is that equations 3.29 and 3.30 are only exactly true at infinite Reynolds and Peclet numbers (Wosnik and George (1994)). At finite value residual effects of the neglected terms remain.

-$\overline{v_yv_x}$, -$\overline{v_xv_z}$ and -$\overline{v_yv_z}$ are the turbulent stresses and -$\overline{v_y\theta}$ and -$\overline{v_x\theta}$ are the turbulent heat fluxes. These terms are the reason why turbulent flows are difficult. With these non-linear fluctuating terms there are more unknown variables than equations. This is referred to *the turbulence closure problem*. The turbulent stress and heat flux terms often have to be modelled when performing numerical computations.

3.4.2 The thermo-viscous and conductive sublayer

The region closest to the wall is called the near wall region. It can be divided into two parts, the buoyant sublayer and the thermo-viscous and conductive sublayer. In the thermo-viscous and conductive sublayer, the sublayer closest the wall, are viscous forces important in the momentum equations and conduction is important in the energy equation. The momentum equations and the energy equation must then have at least one viscous and one conduction term, respectively. In order to get this the governing equations must be rescaled with inner length scales, $\eta\sim\nu/V_{Si}$ and $\eta_t\sim\alpha/V_{Si}$, which have to be sufficiently small relative to δ, i.e the Reynolds and Peclet numbers based on these inner length scales should be of

order unity. V_{Si} and Θ_{Si} are the scaling quantities for the mean temperature and velocities in inner variables. For scaling of fluctuating temperature and velocities are θ_{Si} and v_{Si} used. The continuity equation is the same as in equation 3.28 and the momentum equation and the energy equation becomes then

Equation of momentum in vertical direction

$$0 \simeq \frac{\partial}{\partial y}\left(\nu\frac{\partial V_x}{\partial y} - \overline{v_x v_y}\right) + g\beta(\Theta - \Theta_\infty) \tag{3.35}$$

Equation of energy

$$0 \simeq \frac{\partial}{\partial y}\left(\alpha\frac{\partial \Theta}{\partial y} - \overline{v_y \theta}\right) \tag{3.36}$$

with the following boundary conditions at y = 0

$$V_x = 0 \tag{3.37}$$

$$\Theta = \Theta_w \tag{3.38}$$

$$-\overline{v_x v_y} = 0 \tag{3.39}$$

$$-\overline{v_y \theta} = 0 \tag{3.40}$$

Equations 3.35 and 3.36 can be integrated with respect to y. The integrated x-momentum equation becomes

$$\nu\frac{\partial V_x}{\partial y} - \overline{v_x v_y} + \int_0^{y'} g\beta(\Theta - \Theta_\infty)dy' \cong \nu\left(\frac{\partial V_x}{\partial y}\right)_{y=0} \equiv \frac{\tau_w}{\rho} \equiv u_\star^2 \tag{3.41}$$

where τ_w is the wall shear stress and $u_\star$ is the friction velocity. The inner layer can not be a constant stress layer because of the presence of the integral of the buoyancy force term, except probably at infinite Grashof number. Whether the buoyancy term remain in this limit is not clear. George and Capp (1979) and Wosnik and George (1994) assume it does. Recently however, there are theoretical arguments that it does not (George 2003). An issue is whether $g\beta$ must be included as a scaling parameter in the inner region or not. The integrated energy equation becomes

$$\alpha\frac{\partial \Theta}{\partial y} - \overline{v_y \theta} \cong \alpha\left(\frac{\partial \Theta}{\partial y}\right)_{y=0} \equiv -\frac{q_w}{\rho c_p} \equiv -F_0 \tag{3.42}$$

where q_w is the wall heat flux, α is the thermal diffusivity and F_0 is the kinematic wall heat heat flux. From equation 3.42 the heat flux can be concluded to be constant across the inner layer and that it is independent of the radial distance.

3.4.3 The buoyant sublayer

There is a flow region at the outside of the the inner layer where viscous and conduction terms are losing their importance. This region can also be seen as the inside of the outer flow region. This region is called the buoyant sublayer. For this region the only terms in the reduced equations that remain are the ones that are common for both the outer and the inner flow regions. The continuity equation is the same as 3.28 and the x-momentum equation and energy equation becomes

Equation of momentum in vertical direction

$$0 \simeq -\frac{\partial\overline{(v_x v_y)}}{\partial y} + g\beta(\Theta - \Theta_\infty) \tag{3.43}$$

Equation of energy

$$0 \simeq -\frac{\partial\overline{(v_y \theta)}}{\partial y} \tag{3.44}$$

From equation 3.43 and 3.44 it is clear that the Reynolds' stress is continuously modified by the buoyancy term and that the heat flux in this region is almost constant. As noted above for the viscous sublayer, whether buoyancy should be included here is also an issue (George 2003).

3.5 Heat transfer

Heat transfer is one of the most important things in industrial fluid mechanics. Problems involving both minimizing heat transfer, include heat losses from pipes, and maximizing heat transfer and cooling of electronic components. Heat transfer can be divided into thermal radiation, conduction and convection. Thermal radiation is energy emitted by matter that is at finite temperature, and conduction can be viewed as the transfer of energy from more energetic to less energetic particles of a substance due to interactions between particles. As should have been understood from previous discussions, the focus in this project is on convective heat transfer. In convective heat transfer is energy transferred both by random molecular motion (diffusion), and macroscopic motion of the fluid. Often the term advection is used for macroscopic fluid motion and convection for cumulative transport. Contribution from diffusion dominates closer to the wall but the macroscopic fluid motion becomes more important as the boundary layer grows. As mentioned in sec. 3.1 the heat transfer rate increases when a flow becomes turbulent compared to laminar flows. This means that if the problem is to minimize the heat transfer one should avoid getting transition to turbulence. If one wants to maximize the heat transfer one should instead promote turbulence.

Heat transfer laws are commonly given in terms of a local Nusselt number (dimensionless heat transfer coefficient). For engineering situations it is often some kind of average value of the heat transfer that is wanted. This gives a prediction of the overall heat transfer. A scientist instead, is more interested in the local heat transfer rate for investigation of flow structures. For a laminar boundary layer, with constant wall temperature, the relation $Nu_x \propto Gr_x^{\frac{1}{4}}$ is found from exact solutions of the boundary layer equations (Ostrach (1953)). The relation is based on a vertical length scale. For a turbulent boundary layer there is no exact solution and different suggestions for the relation is often found in the literature. Engineers tries to improve their computational models by changing constants in formulas so it suits their flow cases better. This works for engineering purpose but it will not give a general solution and understanding of the problem. The relation that is mostly accepted is the one from George and Capp (1979). They matched the scalings for the temperature profiles for inner and outer regions and achieved the following formula for constant wall temperature.

$$Nu_x = f(Pr)H_x^{\frac{1}{3}} \tag{3.45}$$

where 'f' is a function of the Prandtl number and H_x is referred to "the H-number" and H_x is defined as $Gr_x \times Nu_x \times Pr^2$. The heat transfer is independent of the vertical distance x. It has been shown by Wosnik (1994) and Wosnik and George (1994) that this equation is only valid at infinite Reynolds number. In practice is a Reynolds number of $10^3 - 10^4$, based on the outer length scale, needed to reach this infinite limit. This mean Grashof numbers about $10^8 - 10^{12}$ or larger. The physical reason for this is that at finite Reynolds number occurs the dissipation over the entire energy spectrum, due to the fact that the energy containing and dissipation wave number are not separated. For finite numbers, which are the cases for laboratory measurements and engineering problems, the heat transfer retain its x-dependence. It is instead dependent on the boundary layer growth and the local Reynolds number.

3.6 Mixed convection

Besides of pure buoyancy-driven flows there can also be buoyancy-driven flows that are affected by a pressure gradient that is due to the free stream velocity. This is said to occur when $Gr/Re^2 \approx 1$ and these flows are called mixed convection flows. This means that both equations for natural convection and forced convection must be used and makes it very hard to deal with theoretical. There are very few theoretical papers dealing with mixed turbulent convection. The boundary conditions will also be different. For example, the free stream velocity does not equal zero at infinity, but instead equals the free stream speed. One can not exclude the buoyancy terms, as for forced convection, and on the other hand can they not be kept fully, as in case of natural convection. The DNS data used in

the present study for analyzing buoyancy-driven boundary layer flows are from a mixed convection case.

Chapter 4

Coherent structures and POD

In this chapter will a discussion about coherent structures be given. Equations for the proper orthogonal decomposition, POD, of a velocity field will also be provided. The focus is put on a variant called "snapshot POD". The energy distribution and reconstruction of velocity components will be shown.

4.1 Coherent structures

In the present work one of the tasks was to investigate the turbulent structures in buoyancy-driven boundary layers. When investigating how the turbulence is created and transferred, much of the work found in the literature was focused on looking for different kind of vortex structures. These are frequently called coherent structures. The problem with this concept is that there is no universal definition of vortex or coherent structures, which makes the whole idea very vague. For example Robinson (1991) defines a coherent motion as *a three-dimensional region of the flow over which at least one fundamental flow variable (velocity component, density, temperature, etc.) exhibits significant correlation with it self or with another variable over a range of space and/or time that is significantly larger than the smallest local scales of the flow.* From this definition one can more or less say that a coherent structure is any by some arbitrary mean identifiable structure in the flow. The main reasons for studying coherent structures are to

- aid predictive modeling of the statistics of turbulent flows.
- make it easier to control turbulence.
- try to understand the dynamical phenomena that occur in the flow.

Frequently, a pressure minimum is used as a detection criterion for a vortex core. There are two things that makes this definition inconsistent. First, there can be unsteady straining, which can create a pressure minimum without involving a vortical motion or swirling motion. Second, viscous effects can eliminate the pressure minimum in a flow with vortical motion. Jeong and Hussain (1995)

proposed another method which removes the above effects. This method will be used in the present study. The information on local pressure extrema is contained in the Hessian of pressure ($\frac{\partial^2 \mathbf{p}}{\partial \mathbf{x}^2}$). A Hessian is a matrix of second partial derivatives of a function, in this case pressure. An equation involving the Hessian of pressure can be obtained by taking the gradient of the momentum equations which gives

$$\frac{\partial \mathbf{a}}{\partial \mathbf{x}} = -\frac{1}{\rho}\frac{\partial^2 \mathbf{p}}{\partial \mathbf{x}^2} + \nu \frac{\partial^3 \mathbf{v}}{\partial \mathbf{x}^3} \tag{4.1}$$

where the left hand side is the acceleration gradient. Note that the Hessian of the pressure is symmetric. The left hand side can be decomposed into symmetric and antisymmetric parts as

$$\frac{\partial \mathbf{a}}{\partial \mathbf{x}} = \underbrace{\left[\frac{D\mathbf{S}}{Dt} + \mathbf{\Omega}\cdot\mathbf{\Omega} + \boldsymbol{S}\cdot\boldsymbol{S}\right]}_{symmetric} + \underbrace{\left[\frac{D\mathbf{\Omega}}{Dt} + \mathbf{\Omega}\cdot\boldsymbol{S} + \boldsymbol{S}\cdot\mathbf{\Omega}\right]}_{antisymmetric} \tag{4.2}$$

The antisymmetric part is the vorticity equation, while the symmetric part is

$$-\frac{1}{\rho}\frac{\partial^2 \mathbf{p}}{\partial \mathbf{x}^2} = \frac{D\mathbf{S}}{Dt} - \nu\frac{\partial^2 \mathbf{S}}{\partial \mathbf{x}^2} + \mathbf{\Omega}\cdot\mathbf{\Omega} + \boldsymbol{S}\cdot\boldsymbol{S} \tag{4.3}$$

where $\frac{D}{Dt}$ is the material derivative, $\mathbf{S}$ is the strain-rate tensor and $\mathbf{\Omega}$ is rotation tensor. The first term on the right hand side of equation 4.3 is the unsteady straining and the second term contains the viscous effects. These two terms will be omitted according to the above method by Jeong and Hussain (1995). Only $\mathbf{\Omega}\cdot\mathbf{\Omega} + \boldsymbol{S}\cdot\boldsymbol{S}$ will be considered for determination of a local pressure minimum. The definition in this case for a vortex core is *a connected region with two negative eigenvalues of* $\mathbf{\Omega}\cdot\mathbf{\Omega} + \boldsymbol{S}\cdot\boldsymbol{S}$. Since this expression is symmetric it has only real eigenvalues. Another fact is that in a plane, the requirement for a local pressure minimum are two positive eigenvalues of the Hessian of pressure (Jeong and Hussain (1995)). From this is the definition for a vortex core that the second eigenvalue should be negative. This is the definition that will be used in the present study for visualization of turbulent structures.

4.2 Proper orthogonal decomposition

Above was a technique to visualize vortex structures given. Another way to investigate the turbulent structures is to use a technique called Proper Orthogonal Decomposition (POD). This was introduced into the fluid dynamic field by Lumley (1967). From now on will $(\cdot)$ and $(\cdot')$ mean (x, y, z, t) and (x', y', z', t'), respectively. The basic idea is as follows. Take a four dimensional, random, vector field $\mathbf{v}(\cdot)$. Seek a deterministic vector field $\boldsymbol{\phi}(\cdot)$ which has the maximum projection on the random field, $\mathbf{v}(\cdot)$, in a mean square sense. Another way to describe it is to find a

deterministic field, $\boldsymbol{\phi}(\cdot)$, for which $\overline{\mid \boldsymbol{\gamma} \mid}^2 = <\mid \mathbf{v}, (\cdot)\boldsymbol{\phi}(\cdot) \mid^2>$ is maximized. If $\mathbf{v}(\cdot)$ and $\boldsymbol{\phi}$ is defined on a Hilbert space, then the inner product can be defined as

$$(\mathbf{v}, (\cdot)\boldsymbol{\phi}^*(\cdot)) = \boldsymbol{\gamma} = \int \int \int_V \mathbf{v}(\cdot)\boldsymbol{\phi}(\cdot)^* d(\cdot) \tag{4.4}$$

asterisk means complex conjugate. If calculus of variation is applied, then the right choice of $\boldsymbol{\phi}(\cdot)$ to maximize $<\mid \boldsymbol{\gamma} \mid^2>$ is a solution to the integral equation

$$\int_\Omega \mathbf{R}(\cdot, \cdot')\boldsymbol{\phi}(\cdot')d(\cdot') = \lambda\boldsymbol{\phi}(\cdot) \tag{4.5}$$

where $\mathbf{R}(\cdot, \cdot')$ is the two-point correlation function defined as

$$\mathbf{R}(\cdot, \cdot') \equiv \overline{\mathbf{v}(\cdot)\mathbf{v}^T(\cdot')} \tag{4.6}$$

Here, a variant of the POD technique, called "snapshot POD", will be used. The original POD is more suitable for high temporal resolution and low spatial resolution, as in case of hot-wire measurements. The "snapshot POD" is preferred when one have high spatial resolution but low temporal resolution, like PIV measurements (Pedersen 2003). In the case of DNS data one can choose which one to use but, as will be seen later, the "snapshot POD" is more computationally efficient. The "snapshot POD" was first derived by Sirovich (1987). When performing a POD the data must be to be uncorrelated, in practice separation two times the integral scale in times ensures this. If number of samples are large, the two-point space-correlation tensor becomes approximately

$$\mathbf{R}(\cdot, \cdot') = \frac{1}{N}\sum_{l=1}^{N} \mathbf{v}_l(\cdot)\mathbf{v}_l^T(\cdot') \tag{4.7}$$

where k and l are the realization number, i.e. different time steps. N is the total number of realizations and T denotes transpose. Assume that the basis modes can be written as

$$\boldsymbol{\Phi}(\cdot) = \sum_{k=1}^{N} A_k(\cdot)\mathbf{v}_k(\cdot') \tag{4.8}$$

then equations 4.7 and 4.8 together with equation 4.5 gives

$$\int_\Omega \frac{1}{N}\sum_{l=1}^{N} \mathbf{v}_l(\cdot)\mathbf{v}_l^T(\cdot')\sum_{k=1}^{N} A_k(\cdot)\mathbf{v}_k(\cdot')d(\cdot') = \lambda\sum_{k=1}^{N} A_k(\cdot)\mathbf{v}_k(\cdot) \tag{4.9}$$

Equation 4.9 can be rewritten as

$$\sum_{k=1}^{N}\left(\frac{1}{N}\int_\Omega \mathbf{v}_l^T(\cdot')\mathbf{v}_k(\cdot')d(\cdot')\right)A_k(\cdot) = \lambda A_l(\cdot) \tag{4.10}$$

This can be written as an eigenvalue problem, which in matrix form can be expressed as

$$\mathbf{CA} = \lambda \mathbf{A} \tag{4.11}$$

$\mathbf{A}$ is now $A_{k,l}$ and equation 4.11 is the same as equation 4.10, but for all l. When solving the eigenvalue problem given by equation 4.11 the result is N orthogonal eigenvectors and corresponding eigenvalues. The eigenvectors can be used to obtain the basis modes in equation 4.8.

$$\mathbf{\Phi}_k(\cdot) = \frac{\sum_{l=1}^{N} A_{k,l}\mathbf{v}_l(\cdot)}{\left\| \sum_{l=1}^{N} A_{k,l}\mathbf{v}_l(\cdot) \right\|} \tag{4.12}$$

Equation 4.12 has been normalized to obtain an orthonormal basis. The above equations are for continous data, but in practice the data are discrete. The discretized eigenvalue problem 4.11 can be written as

$$\hat{\boldsymbol{C}}\boldsymbol{A}_k = \lambda_k \mathbf{A}_k \tag{4.13}$$

where $\hat{\mathbf{C}}$ is calculated as

$$\hat{\mathbf{C}} = \mathbf{v}^T\mathbf{v} \tag{4.14}$$

In the same way can the discretized eigenvalue problem for classical POD be written as

$$\hat{\boldsymbol{R}}\boldsymbol{\phi}_k = \lambda_k \boldsymbol{\phi}_k \tag{4.15}$$

where $\hat{\mathbf{R}}$ is calculated as

$$\hat{\mathbf{R}} = \mathbf{v}\mathbf{v}^T \tag{4.16}$$

The size of matrix $\hat{\mathbf{C}}$ is $N \times N$ while $\hat{\mathbf{R}}$ has size $mno \times mno$. For the present study, m is number of velocity components used and n and o are number of points in the two dimensional spatial domain. From this can be seen that there is a huge reduction in computational cost for "snapshot POD" if one have high spatial resolution but not high temporal resolution. For the DNS data used in the present study, $N$is 126 and mno is about 30 000. The eigenvalue problem is solved and the eigenvalues are ordered according to their size, largest first. The eigenvectors from equation 4.13 can be used for constructing the POD modes according to equation 4.12. The POD modes for the "snapshot POD" becomes

$$\boldsymbol{\phi}_k = \frac{\sum_{l=1}^{N} A_{k,l}(\cdot)\mathbf{v}_l(\cdot)}{\left\| \sum_{l=1}^{N} A_{k,l}(\cdot)\mathbf{v}_l(\cdot) \right\|} \tag{4.17}$$

The original velocity field can be reconstructed by expanding it in series using the POD basis. The original velocity field is projected onto the POD basis and thus

are the expansion coefficients, POD coefficients, determined. The expansion for the discrete case is

$$\mathbf{v}_l = \sum_{k=1}^{N} b_{k,l}\boldsymbol{\phi}_k = \boldsymbol{\Psi}\mathbf{b}_n \tag{4.18}$$

where $\boldsymbol{\Psi} = [\boldsymbol{\phi}_1 \cdots \boldsymbol{\phi}_N]$

$$\mathbf{b}_l = \boldsymbol{\phi}_l^T \mathbf{u}_l \tag{4.19}$$

One of the most important features of POD is that the eigenvalues are a measure of the turbulent kinetic energy. The largest eigenvalue and corresponding basis mode can be used to describe the most energetic structures of the velocity field. The total turbulent kinetic energy is given by the sum of all eigenvalues.

Chapter 5

The computational geometry

The data that will be used for analyzing the turbulent structures are from a direct numerical simulation (DNS). It is important later, when drawing conclusions, to know the conditions for the computation. For a detailed description of the numerical part, see Davidson et al. (2003). The basic idea of DNS is to solve the governing equations at sufficiently high temporal and spatial resolution that everything in the flow can be considered as resolved and turbulence models are not used. The problem with DNS is that it requires a large computer capacity and today is it not possible to use DNS for complex flow cases and one is limited to small time and space domains. The flow case under consideration here is fully developed mixed convection in a vertical channel. The geometry can be found in figure 5.1. One wall is hot, ($\Theta = 1$), and the other wall is cold, ($\Theta = 0$). The dimensionless height (H) is 8π, the width (W) is 2 and the depth (D) is 2π. In x- and z-directions are periodic boundary condition applied, i.e. what goes in must also go out. The z-direction it not physical bounded, only in the computational geometry, and that is why the dashed lines are used. Because this is a mixed convection flow, both the Reynolds and Grashof numbers are important. The Reynolds number $Re_\tau = \frac{u_\star H/2}{\nu} = 150$, where $u_\star$ is the friction velocity (which in this case equals unity). The Grashof number equals 7.68×10^6. These values are low, which means that there is no scale separation between inner and outer length scales. This imply that the asymptotic theory will not be valid for this simulation.

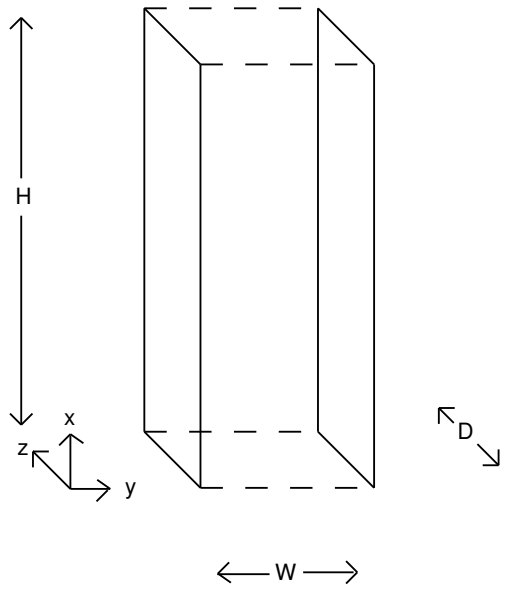

Figure 5.1: *The computational geometry*

Chapter 6

Results

6.1 Results from the visualization

The visualization was performed on the above DNS data for 114 time steps. The second largest eigenvalues were calculated using a FORTRAN code. The visualization was made in TECPLOT. Iso-surfaces for all negative second eigenvalues are used in the analysis. The reason for performing this investigation of turbulent structures is to investigate if this flow field contains vortex structures that takes the form of a horseshoe, so called horseshoe vorticies. If this is the case, it is believed that the simulation has high enough Grashof/Reynolds number to capture these structures. From figure 6.1 one can identify some horseshoe structures. In the left figure is the horseshoe structure located closer to the hot wall than in the right. The right figure is from a later time step than the left figure. The figures are only part of the whole computational geometry.

6.2 Results from the POD analysis

The POD computations were made in MATLAB. The mean velocities were subtracted from the instantaneous velocities to get the fluctuations. These fluctuations were arranged in a vector instead of a matrix. All velocity components were placed in the same vector, which makes the computation efficient. As mentioned in chapter 4, POD gives an estimate of the energy distribution for different sizes of the structure. In figure 6.2 is the energy distribution for the first 50 modes shown. All three velocity components have been used in the left figure. One can se that the largest structures contains less than 7 % of the total kinetic energy. This is a very low value compared to results from other flow cases, for example Johansson (2002). It should also be mentioned that it only affected the result slightly if one, two or all three velocity components were used. In the left part of figure 6.2 is only the streamwise fluctuating velocity component used. The first mode contains in this case about 9 % of the total kinetic energy. Further, the energy decrease with smaller and smaller structures, but not as rapidly as expected. As has been

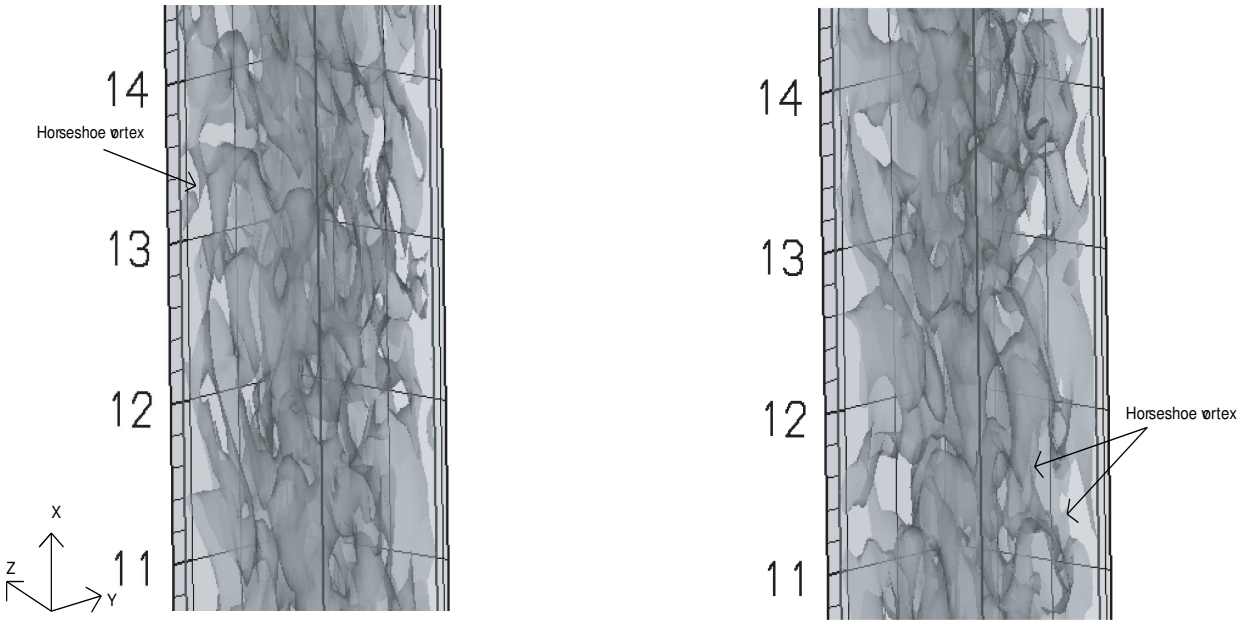

Figure 6.1: *Visualization of vortex structures for part of the computational geometry. Right figure is for a later time step than the left figure. In both figures can horseshoe structures be identified*

reported for other flow cases the POD analysis has shown that the most energy is contained in only the first modes and the rest can be neglected (Johansson 2002). This can not be done in this case. All modes seem to be important. This can be seen when a reconstruction of the velocity field is made. In figure 6.3 is the fluctuating streamwise velocity component for 3 and 50 modes for one time step shown. They are both compared with the original velocity field. It is plotted for a position in the middle of the geometry (x-direction) and across the whole geometry. With only three modes the reconstruction is quite poor. The velocity does not even have the same sign. When using 50 modes, the reconstruction is more similar to the original velocity field. Their can be a couple of explanations why these results appear. One possible explanation could be that 126 snapshots are to few to give an accurate statistical independent analysis. This is a problem when using DNS data. One gets a huge amount of data and it takes long time to calculate it. For example, these 126 snapshots took about 80 hours to calculate and generated about 2 gigabyte of data. Another reason can be due to the cyclic boundary conditions and the flow case it self. In Figure 6.4 are the instantaneous velocity vectors (streamwise and cross-stream) for a certain time

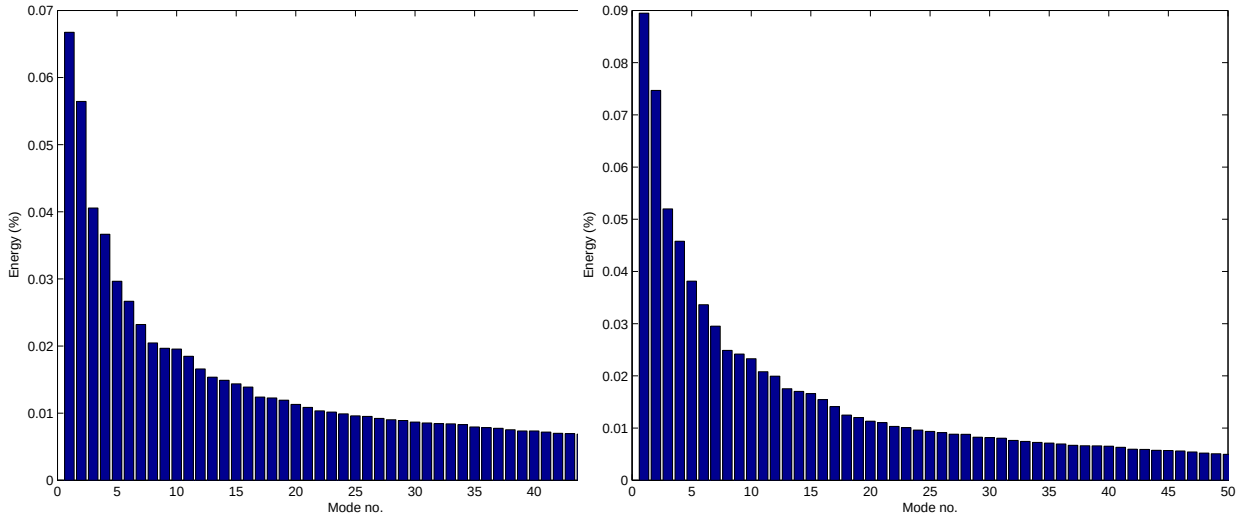

Figure 6.2: *The energy distribution for the first 50 modes. Left: All fluctuating velocity components used. Right: Only the streamwise component used.*

step shown. From this figure it can be argued that the flow field in x-direction is periodic which means that the "snapshot POD" should not be used directly. It seems that the periodic boundary conditions makes the solution not physically a real solution. The velocities have to be Fourier transformed in these directions before doing the POD analysis. This will make the POD computations much more time consuming. A comparison was performed to see what happens to the POD analysis if correlated data was used instead of the uncorrelated data. Number of snapshots were about the same. From this was found that the first mode contained about 27 % of the energy, see figure 6.5. This is a result that was expected from the uncorrelated data also. This does not mean that correlated data should be used for this kind of analysis. It probably only means that to few correlated data were used, so the physical time was very short, and because of that nothing significant happened with the flow during the analysis.

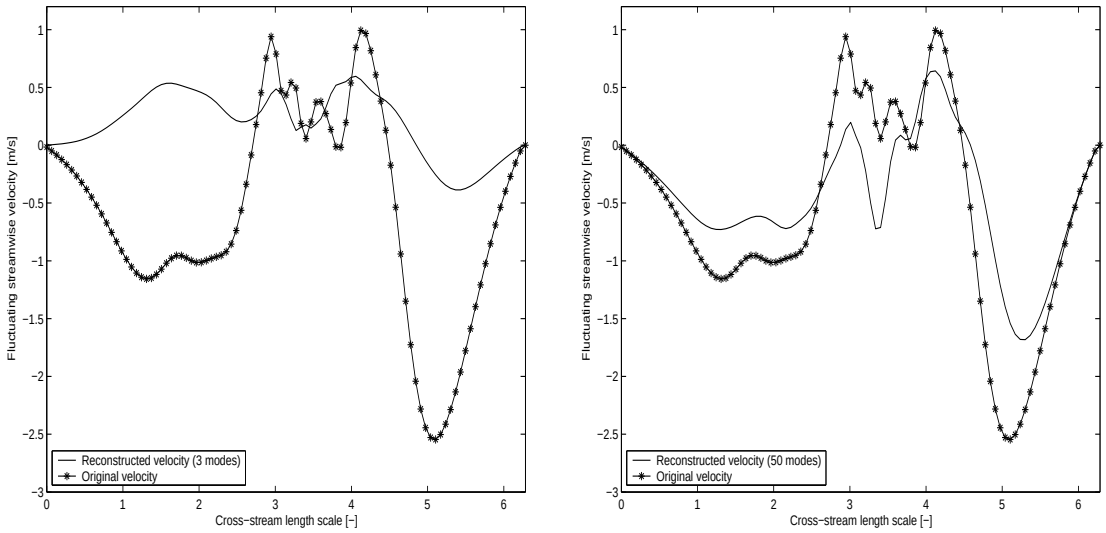

Figure 6.3: *Comparison between the original streamwise velocity fluctuations and the reconstructed. In the left figure has three modes been used and in the right has 50 modes been used.*

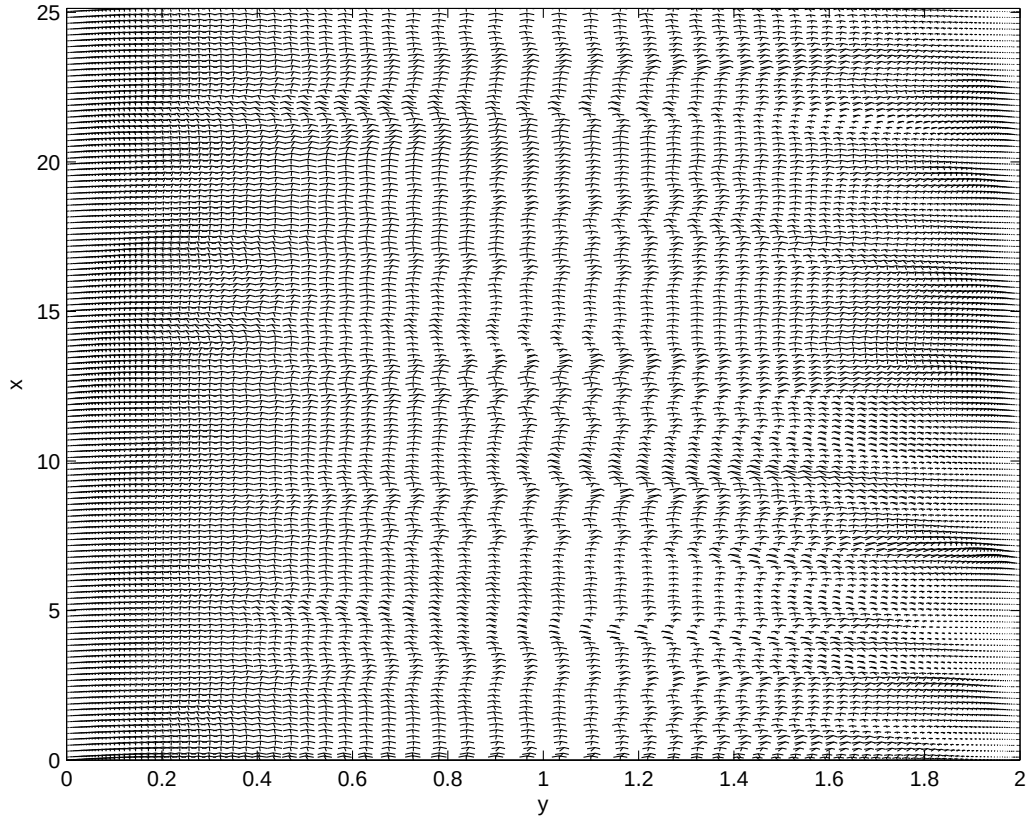

Figure 6.4: *The instantaneous velocity field for the streamwise and cross-stream velocity component for a certain timestep.*

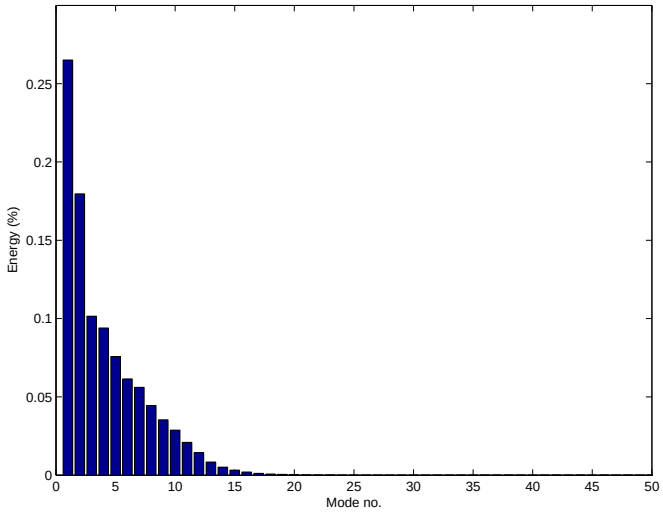

Figure 6.5: *The energy distribution for the first 50 modes using correlated data.*

Chapter 7

Concluding remarks

In this master thesis has an investigation been made on boundary layers caused by buoyancy-driven flows. A literature review was performed and an analysis of the turbulent structures in the flow was performed. It is obvious from the literature that a new large-scale experiment is needed to verify the theories, especially at large Grashof number. From the visualization it is found that this flow case has so called horseshoe structures. From the POD analysis is it clear that more work should be spend on that technique for this flow case. The energy distribution was found to be different from other flow cases.

7.1 Future work

Besides assembling of the experimental facility and initial measurements it is suggested that more attention is paid to the POD analysis of the flow case. This should be done rather than analyzing coherent motions based on pressure minimum criteria, because the pressure minimum criteria is very vague and there is no universal definition. The following ideas should be tested to improve the POD results.

- Make a Fourier transform in the seemingly periodic directions.

- Use larger amount of uncorrelated samples in the analysis

A natural continuation of the POD analysis is to perform it on measurements as well as on DNS data. This will give an answer to if the results are due to boundary conditions or something else related to the computations, or if the difference in energy is small between the different modes for this kind of flow.

Bibliography

Barhaghi, D.G., Davidson, L. and Karlsson, R. (2002) *Natural convection heat transfer in a vertical shell and tube.* Internal report 03/01, Chalmers university of technology, Gothenburg.

Camargo, R., Luna, E. and Trevino, C. (1996) Numerical study of the natural convective cooling of a vertical plate. *Heat and Mass Transfer,* Vol. 32, 89-95. ISSN 0947-7411

Cheesewright, R. and Ierokipiotis, E. (1982) Velocity measurements in a turbulent natural convection boundary layer. *Proc. of seventh International Heat Transfer Conference*, Vol. 2, Munich, Sep 06-10 1982, Grigull, U., Hahne, E., Stephan, K. and Straub, J. (Eds.), 305-309. ISBN 0-89116-342-5

Davidson, L., Čuturić, D. and Peng, S.-H. (2003) DNS in a plane vertical channel with and without buoyancy. *Proc. of fourth International Symposium on Turbulence, Heat and Mass Transfer*, Antalya, Oct 12-17 2003, Hanjalić, K., Nagano, Y. and Tummers, M. (Eds.)

George, W.K. (2003) *Private communication.* Div. Thermo and Fluid Dynamics, Chalmers University of Technology, Gothenburg, Sweden.

George, W.K. and Capp, S.P. (1979) A theory for natural convection turbulent boundary layers next to heated vertical surfaces. *Int. J. Heat Mass Transfer*, Vol. 22, 813-826. ISSN 0017-9310

Heist D.K. and Castro I.P. (1998) Combined laser-doppler and cold wire anemometry for turbulent heat flux measurement. *Experiments in fluid,* Vol. 24, 375-381. ISSN 0723-4864

Hoogendorn, C. J. and and Euser, H. (1978) Velocity profiles in the turbulent free convection boundary layer. *Proc. of the sixth International Heat Transfer Conference*, Vol. 2, Toronto, 193-198. ISBN 0-89116-135-X

Ierokipiotis, E.G. (1983) The study of the development of a natural convection boundary layer using Laser-Doppler Anemometry. Ph. D. Thesis, Queen Mary College, London

Incropera, F.P. and DeWitt, D.P. (2002) *Fundamentals of heat and mass transfer* (5.ed.) New York: John Wiley & Sons. ISBN 0-471-38650-2

Jeong, J. and Hussain, F. (1995) On the identification of a vortex. *J. Fluid Mech.*, Vol. 285, 69-94. ISSN 0022-1120

Johansson, P.B.V. (2002) *The Axisymmetric Turbulent Wake* Ph.D. Thesis, Chalmers University of Technology, Gothenburg, Sweden. ISBN 91-7291-178-6

Kato, S., Murakami, S. and Yoshie, R. (1993) Experimental and numerical study on natural convection with strong density variation along a heated vertical plate. *Ninth Symp. on Turbulent Shear Flows*, Vol 2, Kyoto, Aug 16-18, 12.5.1-12.5.6

Lumley, J.L. (1967) The structure of Inhomogenous Turbulent flows. In: Yaglom, A.M. and Tatarski, V.I (Eds.) *Atmospheric Turbulence and Radio Wave Propagation.* 166-178.

Miyamoto, M., Kajino, H., Kurima, J. and Takanami, I. (1982) Development of turbulence characteristics in a vertical free convection boundary layer. *Proc. of seventh International Heat Transfer Conference*, Vol. 2, Munich, Sep 06-10 1982, Grigull, U., Hahne, E., Stephan, K. and Straub, J. (Eds.), 323-328. ISBN 0-89116-342-5

Morel, T. (1975) Comprehensive design of axisymmetric wind tunnel contractions. *J. Fluids Eng.*, Vol. 97, no 2, 225-233, ISSN 0098-2202

Morel, T. (1977) Design of two-dimensional wind tunnel contractions. *J. Fluids Eng.*, Vol. 99, 371-378, ISSN 0098-2202

Ostrach, S. (1953) An analysis of laminar free-convection flow and heat transfer about a flat plate parallel to the direction of the generating body force. *NACA technical reports*, no 1111, 63-79

Panton, R. (1996) *Incompressible flow.* (2.ed.) New York: John Wiley & sons Inc. ISBN 0-471-59358-3

Pedersen, J.M. (2003) *Analysis of Planar Measurements of Turbulent flows.* Ph. D. Thesis, Technical University of Denmark, Lyngby. ISBN 87-7475-292-8

Persson, N.J. and Karlsson, R.I. (1996) Turbulent natural convection around a heated vertical slender cylinder. *Proc. of eigth International Symposium on Applications of Laser Techniques to Fluid Mechanics*, Lisbon, Jul 08-11 1996

Pietri, L., Amielh, M. and Anselmet, F. (2000) Simultaneous measurements of temperature and velocity fluctuations in a slightly heated jet combining a cold wire and Laser Doppler Anemometry. *Int. J. Heat Fluid Flow,* Vol. 21, 22-36. ISSN 0142-727X

Robinson, S.K. (1991) Coherent motions in the turbulent boundary layer. In: Lumley, J.L., van Dyke, M. and Reed, H.L. (Eds.) *Annu. Rev. Fluid Mech.* Vol. 23, 601-639. ISBN 0-8243-0723-2

Sirovich, L. (1987) Turbulence and the dynamics of coherent structures. Part I: Coherent structures. *Quart. Appl. Math.*, Vol. 45, no 3, 561-571. ISSN 0033-569X

Tagawa, M., Nagaya, S. and Ohta, Y. (2001) Simultaneous measurement of velocity and temperature in high-temperature turbulent flows: a combination of LDV and a three-wire temperature probe. *Experiments in Fluids,* Vol. 30, 143-152. ISSN 0723-4864

Tennekes, H. and Lumley, J.L. (1972) *A first course in turbulence.* Cambridge: MIT Press. ISBN 0-262-20019-8

Tsuji, T. and Nagano, Y. (1988a) Characteristics of a turbulent natural convection boundary layer along a vertical flat plate. *Int. J. Heat Mass Transfer*, Vol. 31, no 8, 1723-1734. ISSN 0017-9310

Tsuji, T. and Nagano, Y. (1988b) Turbulence measurements in a natural convection boundary layer along a vertical flat plate. *Int. J. Heat Mass Transfer*, Vol. 31, no 10, 2101-2111. ISSN 0017-9310

Tsuji, T., Nagano, Y. and Tagawa, M. (1991) Thermally driven turbulent boundary layer. *Eigth Symposium on Turbulent Shear Flows*, Munich, Sep 09-11 1991

Versteegh, T.A.M. and Nieuwstadt, F.T.M. (1998) Turbulent budgets of natural convection in an infinite, differentially heated, vertical channel. *Int. J. Heat Fluid Flow,* Vol. 19, 135-149. ISSN 0142-727X

Wosnik, M. (1994) *Outline of a new theory for the natural convection turbulent boundary layer next to heated vertical surfaces*. M.Sc. Thesis, State university of New York, Buffalo.

Wosnik, M. and George, W.K. (1994) Another look at the turbulent natural convection boundary layer next to heated vertical surfaces. *Proc. ICHMT Symposium on Turbulence, Heat and Mass Transfer*, Lisbon, Aug 09-12 1994, Hanjalic, K. and Pereira, J.C.F. (Eds.), Vol. 1, 14.5.1-14.5.6. ISBN 1-56700-040-1

Appendix A

Boundary layer equations in cylindrical coordinates

In this appendix is the governing equations for a turbulent natural convection boundary layer given in cylindrical coordinates. It follows the same structure as for the cartesian equations in chapter 2. It has been assumed that it is 2-dimensional flow. The x-direction is directed opposite way of the gravitational force and r-direction is the radial direction directed out from the the heated cylinder wall.

The outer region of the boundary layer

Equation of continuity

$$\frac{\partial V_x}{\partial x} + \frac{1}{r}\frac{\partial (rV_r)}{\partial r} = 0 \tag{A.1}$$

Equation of momentum in vertical direction

$$V_x\frac{\partial V_x}{\partial x} + V_r\frac{\partial V_x}{\partial r} \simeq -\frac{1}{r}\frac{\partial \overline{(rv_xv_r)}}{\partial r} + g\beta(\Theta - \Theta_\infty) \tag{A.2}$$

Equation of energy

$$V_r\frac{\partial \Theta}{\partial r} + V_x\frac{\partial \Theta}{\partial x} \simeq -\frac{\partial \overline{(v_x\theta)}}{\partial x} - \frac{1}{r}\frac{\partial \overline{(\theta v_r r)}}{\partial r} \tag{A.3}$$

with the following boundary conditions as r $\rightarrow \infty$

$$V_x = 0 \tag{A.4}$$

$$\Theta = \Theta_\infty \tag{A.5}$$

$$-\overline{v_rv_x} = 0 \tag{A.6}$$

$$-\overline{v_r\theta} = 0 \tag{A.7}$$

The thermo-viscous and conductive sublayer

Equation of momentum in vertical direction

$$0 \simeq \frac{\nu}{r}\frac{\partial}{\partial r}\left(r\frac{\partial V_x}{\partial r}\right) - \frac{1}{r}\frac{\partial\overline{(rv_xv_r)}}{\partial r} + g\beta(\Theta - \Theta_\infty) \tag{A.8}$$

Equation of energy

$$0 \simeq \frac{\partial}{\partial r}\left(\alpha\frac{\partial\Theta}{\partial r}\right) - \frac{1}{r}\frac{\partial\overline{(\theta v_r r)}}{\partial r} \tag{A.9}$$

with the following boundary conditions at r = 0

$$V_x = 0 \tag{A.10}$$

$$\Theta = \Theta_w \tag{A.11}$$

$$-\overline{v_r'v_x'} = 0 \tag{A.12}$$

$$-\overline{v_r\theta} = 0 \tag{A.13}$$

The buoyant sublayer

Equation of momentum in vertical direction

$$0 \simeq -\frac{\nu}{r}\frac{\partial\overline{(rv_xv_r)}}{\partial r} + g\beta(\Theta - \Theta_\infty) \tag{A.14}$$

Equation of energy

$$0 \simeq -\frac{1}{r}\frac{\partial\overline{(\theta v_r r)}}{\partial r} \tag{A.15}$$

Appendix B

Specifications for the proposed experimental facility

In this chapter are some details about the proposed experimental facility provided. Some basic data is summarized in the table below.

Diameter of outer isolating shell	1.2 m
Diameter of the heated cylinder	0.15 m
Height of the heated cylinder	4.5 m
Max. temperature of cylinder	80°C
Max. Grashof number*	4×10^{11}
Working fluid	Air

**According to equation 3.1 with $\Theta_w = 80°C$ and $\Theta_\infty = 20°C$, ν evaluated at the film temperature and with height L=4m.*

The proposed experimental facility (figure B.1) consists of a centrally positioned heated vertical aluminium cylinder that is 4.5 m high and 0.15 m in diameter. The aluminium cylinder is enclosed by a circular shell that is 1.2 m in diameter and an inlet box at the bottom and an outlet box at the top. The reason that the aluminium cylinder is enclosed by a shell is to minimize disturbances from the surrounding and to control the flow. By controlling the temperature and the flow rate of the air around the heated cylinder, the co-flow (a small flow at small height due to mixed convection) can be adjusted to be zero at a certain height. This mean that the thermal stratification can be controlled. The aluminium cylinder is heated with water and the water flow is large so the cylinder can be considered isothermal. Maximum temperature of the cylinder wall is about 80 degrees C, which will give a Grashof number of about 4×10^{11} at height 4 m. The water is heated inside a water tank, which contains about 1 m^3, with electrical heaters. The water tank is placed about 3 meters above the floor to increase the pressure on the suction side of the pump in order to avoid cavitation.

The working fluid is chosen to be air. Air is more suitable than water because

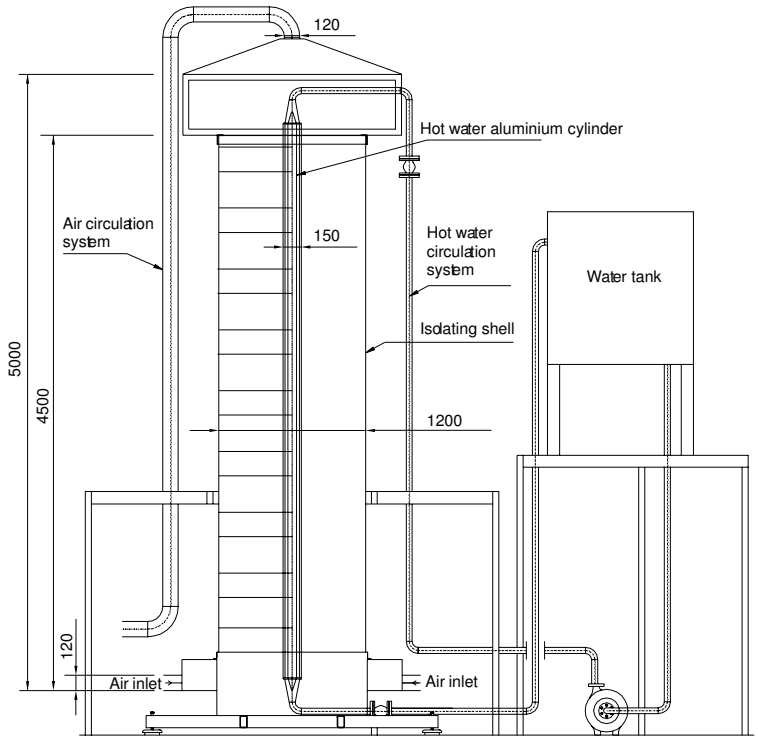

Figure B.1: *A schematic picture of the proposed experimental rig. The values are in mm.*

water has large refraction-index variations due to the variations in density which makes optical methods impossible to use for accurate velocity measurements. It is also easier to work with air than water, i.e. leakage. The air enters the system from inlet pipes in the inlet box. The air flow circulates around the aluminium cylinder and exits through an air collection hood at the top. The air from the outlet passes through a HVAC (Heat, Ventilation and Air Condition) unit and is cooled down. When the air has been cooled down it enters the inlets again. The air should be uniformly distributed around the perimeter so that the inlet flow becomes horizontal and directed radially inwards. This implies that the flow is to be considered as axisymmetric and two-dimensional. This is of great importance because this will specify well-known inlet and outlet boundary conditions, which are one requirement for using the experiment for validation of turbulence models. The outer shell has optical transparent windows to allow Laser based measurement methods, such as LDA (Laser Doppler Anemometry) and PIV (Particle Image Velocimetry), as well as flow visualizations.

Appendix C

Modification of the contraction

As mentioned in chapter 1, the inlet velocity was not sufficiently uniform around the inlet perimeter to be considered axisymmetric. It is believed that this was due to the design of the initial contraction, see figure C.1. Two cases were investigated for the initial design of the contraction. The first measurement was 25 mm over the bottom plate and 5 mm out from the inlet. The second measurement was 25 mm over the bottom plate and 98 mm out from a screen that was placed before the inlet to damp out the velocity fluctuations. In figure C.2 is the radial inlet mean velocity profile shown. These velocities were measured at 32 positions around the inlet perimeter using a pitot-static tube and a sensitive, integrating pressure transducer. In figure C.3 is the deviation from the mean velocity shown for both cases. One can see that there is large deviation from the mean value at many positions. As already pointed out was this the reason for redesigning the contraction. It is hard draw any conclusion whether or not a screen make any improvement in this case. At some positions is the deviation smaller with a screen and at other it is larger.

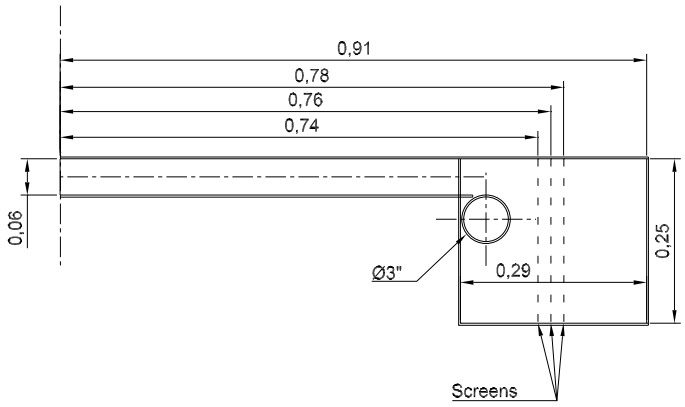

Figure C.1: *The initial contraction with three screens shown. The flow is coming from right. The origin is placed in the center of the inlet section*

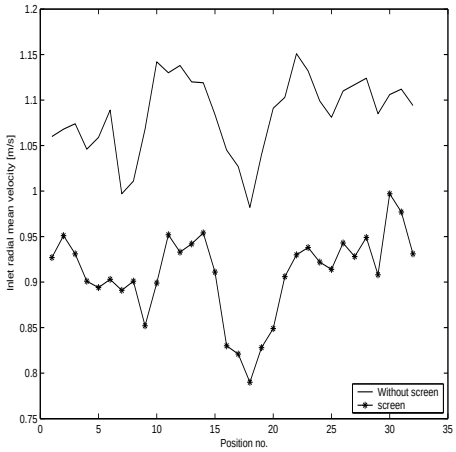

Figure C.2: *The radial inlet mean velocity profile for the initial contraction with and without perforated plate.*

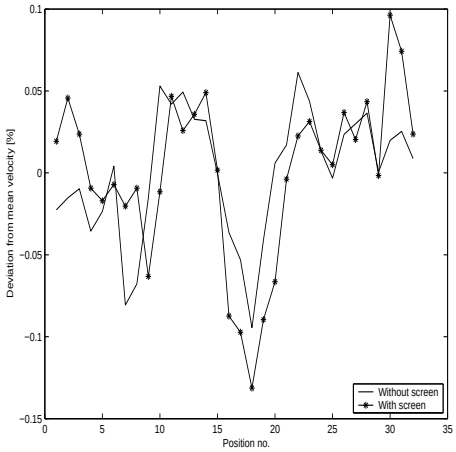

Figure C.3: *The deviation from mean velocity around the perimeter of the initial contraction.*

The contraction was redesigned in order to improve the flow quality. The new contraction is based on the contraction from Morel (1975 and 1977). Too reduce the fluctuations the outlet height for the modified contraction has increased from 50 mm to 120 mm. In figure C.4 is a drawing of the modified contraction. The modified inlet section has, because of that, increased in overall diameter to 3 300 mm (including inlet pipes). More screens has also been added in hope to improve the flow quality. The shape of the contraction is calculated using the two formulas:

$$H_c = H_1 - \frac{H_1 - H_2}{\left(\frac{r_m}{L_c}\right)^2} \frac{r_c^3}{L_c^3} \tag{C.1}$$

for $\frac{r_c}{L_c} \leq \frac{r_m}{L_c}$.

$$H_c = H_2 + \frac{H_1 - H_2}{1 - \left(\frac{r_m}{L_c}\right)^2} \left(1 - \frac{r_c}{L_c}\right)^3. \tag{C.2}$$

for $\frac{r_c}{L_c} > \frac{r_m}{L_c}$.

H_1	0.24 m	Inlet height
H_2	0.06 m	Outlet height
L_c	0.48 m	Contraction length
r_m	0.252 m	Matching point

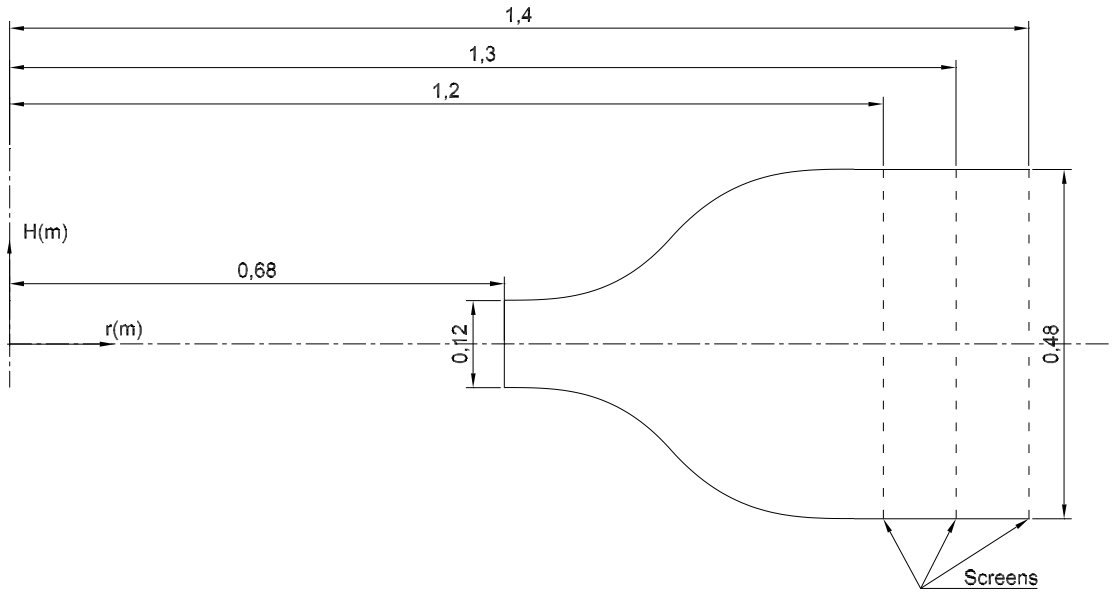

Figure C.4: *The modified contraction with three screens shown. The flow is coming from right. The origin is placed in the center of the inlet section*